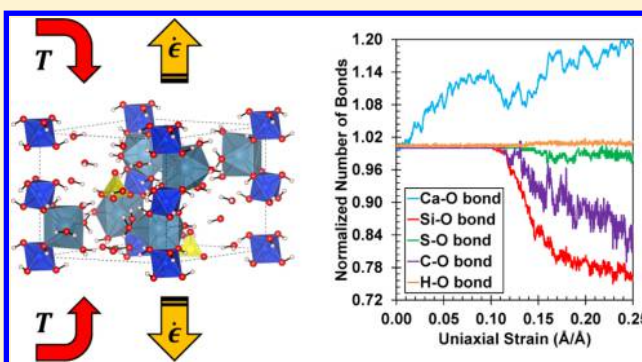


Reactive Molecular Dynamics Simulations to Understand Mechanical Response of Thaumasite under Temperature and Strain Rate Effects

Shahin Hajilar,[†] Behrouz Shafei,^{*,†,‡,§} Tao Cheng,[§] and Andres Jaramillo-Botero^{*,§}[†]Department of Civil, Construction and Environmental Engineering, Iowa State University, Ames, Iowa 50011, United States[‡]Department of Materials Science and Engineering, Iowa State University, Ames, Iowa 50011, United States[§]Chemistry and Chemical Engineering, California Institute of Technology, Pasadena, California 91125, United States

ABSTRACT: Understanding the structural, thermal, and mechanical properties of thaumasite is of great interest to the cement industry, mainly because it is the phase responsible for the aging and deterioration of civil infrastructures made of cementitious materials attacked by external sources of sulfate. Despite the importance, effects of temperature and strain rate on the mechanical response of thaumasite had remained unexplored prior to the current study, in which the mechanical properties of thaumasite are fully characterized using the reactive molecular dynamics (RMD) method. With employing a first-principles based reactive force field, the RMD simulations enable the description of bond dissociation and formation under realistic conditions. From the stress–strain curves of thaumasite generated in the *x*, *y*, and *z* directions, the tensile strength, Young's modulus, and fracture strain are determined for the three orthogonal directions. During the course of each simulation, the chemical bonds undergoing tensile deformations are monitored to reveal the bonds responsible for the mechanical strength of thaumasite. The temperature increase is found to accelerate the bond breaking rate and consequently the degradation of mechanical properties of thaumasite, while the strain rate only leads to a slight enhancement of them for the ranges considered in this study.



1. INTRODUCTION

Thaumasite is a calcium silicate carbonate sulfate hydrate phase, known as the main product and indicator of thaumasite sulfate attack (TSA) in cementitious materials.^{1–4} Cementitious materials exposed to sulfate bearing solutions from the outside environment, such as soil and water, show significant deterioration over time. This occurs through the attack of external sulfate ions to the calcium silicate hydrates (CSH), which are the main binding agents in ordinary and sulfate-resisting Portland cements. As a result of such chemical reactions, thaumasite is precipitated. The formation of thaumasite substantially reduces the binding capacity of the cement paste, transforming it into a mushy and incohesive mass.⁵ In addition, the replacement of CSH with thaumasite can cause significant stresses and strains, leading to the expansion of the paste, formation of cracks, and eventually spalling and degradation of civil infrastructures made of concrete.⁶ While TSA can be destructive at any finite temperature, it has been observed it is greatly accelerated at temperatures below 0 °C.^{7,8} To address the long-standing deterioration issues associated with TSA to cementitious materials, an in-depth understanding of the structural, thermal, and mechanical properties of thaumasite is essential.

Jacobsen et al.⁹ studied the thermal expansion of thaumasite between 130 and 298 K using single-crystal X-ray diffraction. Over this temperature range, no phase transition was observed

and most structural units demonstrated positive thermal expansion coefficients. Moreover, it was revealed that, contrary to the carbonate groups with zero thermal expansions, the sulfate tetrahedra and the silicate octahedra exhibit negative thermal expansions. A high-temperature study of thaumasite was conducted by Martucci and Cruciani.¹⁰ In situ, time-resolved synchrotron power diffraction between 303 and 1098 K was used for this purpose. It was observed that the cell parameters of thaumasite increased linearly with temperature up to 393 K. As a result of the complete removal of the crystallization water molecules, however, the crystalline structure of thaumasite collapsed at close to 417 K, turning it into an amorphous structure. By a further increase of temperature, anhydrite and cristobalite crystallized at 953 K. In a separate effort, the structure of thaumasite was characterized in detail using single-crystal neutron diffraction and Raman spectroscopy by Gatta et al.¹¹ The stability of the structure of thaumasite was attributed to the geometry of hydrogen bonds that connect the main structural units. This study found that by decreasing the temperature, although the hydrogen bonds became shorter, the sulfate tetrahedra expanded, indicating negative thermal expansion at the molecular level driven by shrinkage of the

Received: March 24, 2017

Revised: May 19, 2017

Published: May 22, 2017

hydrogen bonds between the $[\text{Ca}_3\text{Si}(\text{OH})_6\cdot 12\text{H}_2\text{O}]^{4+}$ columns. Most recently, Scholtzová et al.¹² performed Brillouin spectroscopy experiments and ab initio simulations to generate the full elasticity tensor of thaumasite. From the calculated elastic constants, the bulk, shear, and Young's moduli, as well as Poisson's ratio, of thaumasite were estimated. This was the only study, to our knowledge, that characterized the mechanical properties of thaumasite in the elastic range. There is, however, no evidence to understand the expansion, loss of strength, and crack formation observed in thaumasite during the experiments due to TSA. The current study primarily focuses on addressing this critical research gap.

Prior studies have demonstrated the capabilities of the reactive molecular dynamics (RMD) method to calculate the mechanical properties of cementitious crystalline materials.^{13,14} In this study, first-principles based ReaxFF RMD¹⁵ simulations are performed to investigate the mechanical characteristics of thaumasite. The ReaxFF force field is used from Liu et al.,¹³ albeit complemented with C–Ca bond interactions^{16,17} prepared using the GARFIELD parameter optimization framework.¹³ To this end, the crystalline atomistic structure of thaumasite is built and then deformed uniaxially in the *x*, *y* and *z* directions of the simulation cell. In addition to recording the stress–strain data, a chemical bond analysis is performed on the resulting atomistic trajectories to correlate the stretching of chemical bonds with the stresses obtained by the RMD simulations. From the stress–strain curves, the tensile strength, Young's modulus, and fracture strain of thaumasite are determined. In the next step, an extensive set of RMD

simulations are performed to investigate the sensitivity of the mechanical properties of thaumasite to temperature and strain rate effects. From the results generated at a wide range of temperatures and strain rates, the relationships between the tensile strength of thaumasite and these two important factors are identified. The outcome of this study contributes to enhance the understanding of the key mechanical properties of thaumasite under different thermal and loading conditions, which can be further used to develop constitutive models for cementitious materials at various length scales.

2. COMPUTATIONAL DETAILS

Crystalline Structure of Thaumasite. Thaumasite ($\text{Ca}_3\text{Si}(\text{OH})_6(\text{CO}_3)(\text{SO}_4)\cdot 12\text{H}_2\text{O}$) is a rare mineral that has a hexagonal structure with 122 atoms in the unit cell and a space group of $P6_3$. Because more than half of the weight of this crystalline structure is from water and hydroxyl, thaumasite has a relatively low density of 1.88 g/cm³. The crystalline structure of thaumasite (Figure 1) was first determined by Edge and Tylor¹⁸ and later refined by other studies, such as Effenberger et al.¹⁹ and Gatta et al.¹¹ Thaumasite is the only known mineral that possesses silicon atoms coordinated by six hydroxyl groups stable at (or close to) ambient pressure–temperature conditions. Using infrared spectra, Moenke²⁰ was the first study that recognized that thaumasite contains octahedral silicon atoms. It was later confirmed by ²⁹Si NMR spectroscopy that the silicon atoms in thaumasite are six-coordinated.^{21,22} This is a unique feature as other silicate minerals that make up most of the earth's

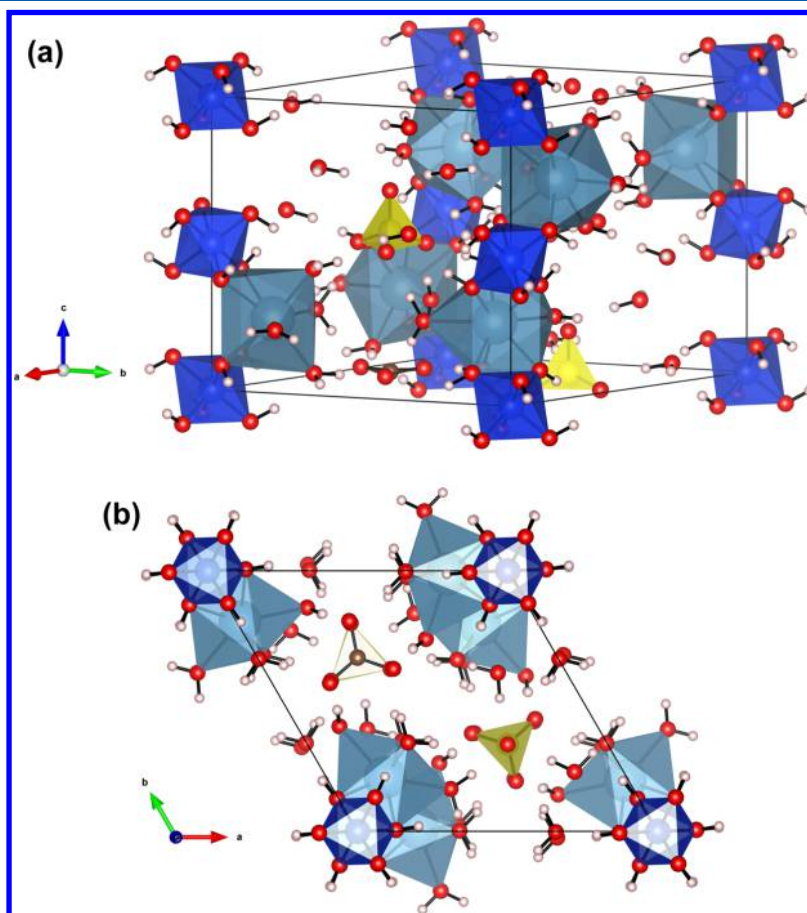
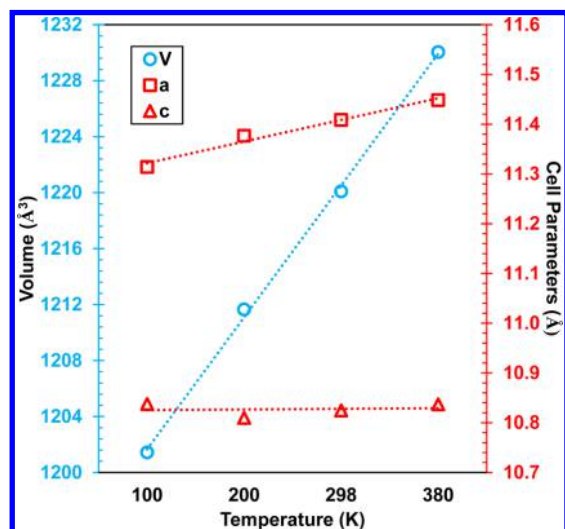


Figure 1. (a) Unit cell of thaumasite and (b) crystal structure of thaumasite viewed from (001). The color scheme is as follows: blue: silicon; cyan: calcium; yellow: sulfur; brown: carbon; red: oxygen; white: hydrogen.

Table 1. Thaumasite Cell Parameters Calculated Using ReaxFF and Obtained by Gatta et al.'s¹¹ Experimental Tests

cell parameters (Å)	ReaxFF NPT-RMD	experiment	difference (%)
<i>a/b</i>	11.4048	11.0545	3.20
<i>c</i>	10.8245	10.4131	3.95

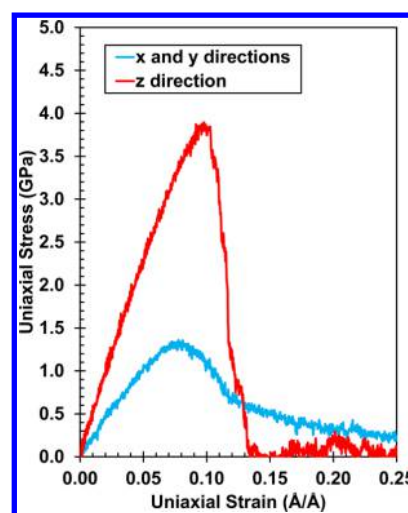
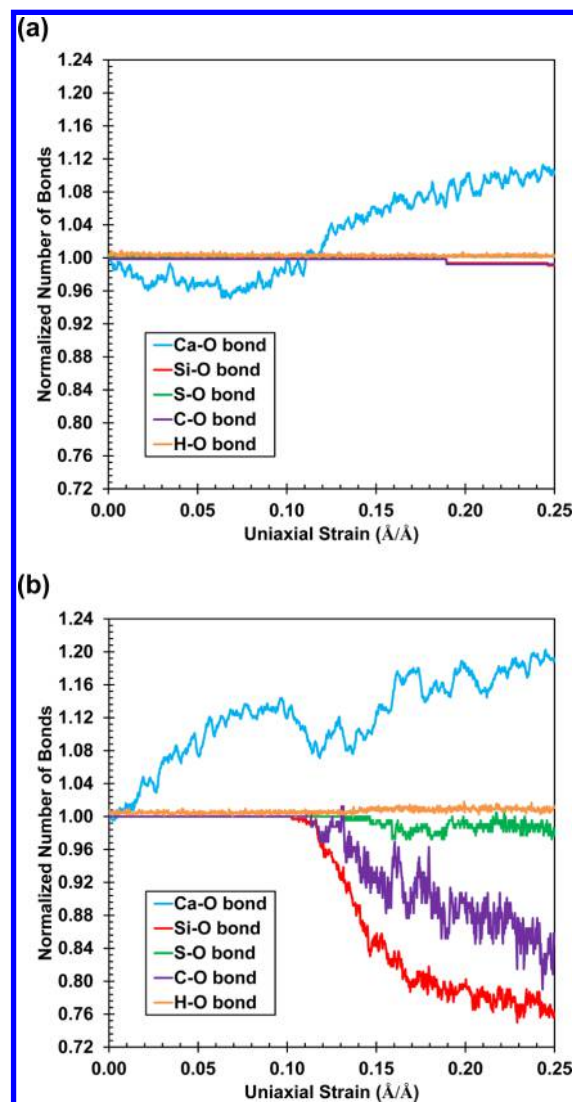
**Figure 2.** Thermal expansion of thaumasite between 100 and 380 K.**Table 2.** Mean Thermal Expansion Coefficients of Thaumasite in Various Temperature Ranges

	100–200 K	200–298 K	298–380 K	100–380 K
$\alpha_V (\times 10^{-5} \text{ K}^{-1})$	8.50	7.10	9.94	8.50
$\alpha_a (\times 10^{-5} \text{ K}^{-1})$	5.53	2.85	4.26	4.24
$\alpha_c (\times 10^{-5} \text{ K}^{-1})$	−2.57	1.39	1.39	−2.54

Table 3. Elastic Properties of Thaumasite Calculated Using ReaxFF and Obtained from Scholtzová et al.'s¹² Experimental Tests

elastic properties	ReaxFF NVT-RMD	experiment
C_{11} (GPa)	41.26	59.9
C_{12} (GPa)	32.88	34.3
C_{13} (GPa)	25.98	24.1
C_{33} (GPa)	65.84	61.4
C_{44} (GPa)	8.77	13.9
C_{66} (GPa)	5.44	12.8
K (GPa)	35.33	38.4
G (GPa)	8.31	14.5
E (GPa)	23.12	38.6
ν	0.39	0.33

crust contain silicon atoms coordinated to four oxygen atoms. The other two silica compounds that contain fully hydrated, six-fold coordinated silicon atoms, however, have been found in the synthetic high-pressure phase D, $\text{MgSi}(\text{OH})_2\text{O}_4$ ^{23,24} and $\text{MgSi}(\text{OH})_6$.²⁵ In thaumasite, six hydroxyl groups are coordinated to Si^{4+} , resulting in $\text{Si}(\text{OH})_6^{2-}$ anions, which are balanced by Ca^{2+} cations. These anions and cations are surrounded by 12 water molecules that form columns of $[\text{Ca}_3\text{Si}(\text{OH})_6 \cdot 12\text{H}_2\text{O}]^{4+}$, which lay parallel to the *c* axis of the unit cell. These columns are interconnected only through hydrogen bonding with the SO_4^{2-} and CO_3^{2-} groups located in the interstitial positions in the channels between the columns. The sulfate and carbonate groups

**Figure 3.** Stress–strain curves of thaumasite under tensile strains in the *x/y* and *z* directions.**Figure 4.** Changes in the number of bonds during the straining of thaumasite in the (a) *x/y* directions and (b) *z* direction.

that neutralize the excess charge of the system alternate along the *c* axis of the unit cell and are fully ordered.

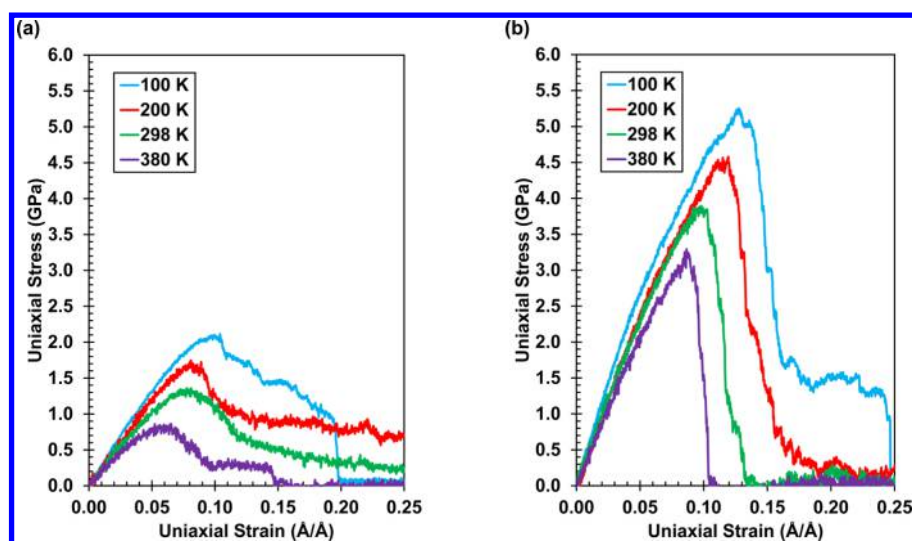


Figure 5. Stress–strain curves of thaumasite at different temperatures under uniaxial tensile strains in the (a) x/y directions and (b) z direction.

Mechanical Properties from RMD Simulations. The RMD simulations are conducted using the large-scale atomic/molecular massively parallel simulator (LAMMPS) package.²⁶ The triclinic unit cell of thaumasite is built in the LAMMPS input format using the latest crystallographic data available in the literature.¹¹ Because thaumasite crystallizes in a trigonal lattice (a , b , and c axes), the simulation cell is generated by extending the unit cell of thaumasite three times in the a , b , and c directions. The simulation cell of thaumasite contains a total of 3294 atoms. The interatomic interactions are described using the ReaxFF force field developed by van Duin et al.¹⁵ ReaxFF partitions the total energy of interactions similar to those found in classical nonreactive force fields, that is, in valence, nonbonded, and H-bond terms, but it introduces bond order dependencies on valence terms and additional potential energy corrections in the form of penalties or contributions to properly describe bond dissociation and formation under different environmental conditions. By using a bond length/order relationship, smooth transitions from nonbonded to single, double, and triple bonded systems, and vice versa, are obtained. Furthermore, charges are allowed to change as bonds are broken or formed. The van der Waals (vdW) interactions are included between all atoms, not just nonbonded ones, which allows the valence bonding interaction to be monotonically attractive. Because the vdW inner wall balances the bond attraction, all valence interactions depend on the bond order and go to zero as the bonds are broken. All parameters are obtained directly and systematically from quantum mechanics. The atomic charges calculated by the charge equilibrium (QEq) method²⁷ are updated at each time step. The ReaxFF parameters used in this study have been derived from Liu et al.¹³ and then extended and reoptimized to include all sulfur interactions using GARFFfield.^{16,17} To ensure the structural stability and conformity of the thaumasite model in ambient conditions, its $3 \times 3 \times 3$ super cell is equilibrated for 100 ps using an isobaric–isothermal (NPT) ensemble at 298 K and 0 atm at a time step of 0.25 fs. The final 50 ps of the equilibrated trajectories are used to compute the cell parameters. Convergence of a variety of parameters, including total energy and its components, lattice parameters, and volume, are particularly monitored and ensured. The equilibrated molecular structure of thaumasite is then used as the initial

configuration for characterization of the stress–strain behavior at both elastic and plastic ranges.

Calculation of Elastic Properties at Finite Temperature and Pressure. The elastic constants of thaumasite are calculated from the linear relation between the stress and strain tensors within the limit of infinitesimal deformation. In this study, the elastic constants are calculated from the $3 \times 3 \times 3$ super cell of thaumasite equilibrated at room temperature (298 K). The simulation cell is then subjected to 12 strain configurations, including three uniaxial tension/compression pairs and three shear pairs. Small deformations for each configuration have been applied to ensure that the strains remain in the elastic range. Each separate straining simulation is performed for 30 ps with a time step of 0.25 fs. The pressure of the system for the last 10 ps dynamics is recorded to obtain the elastic constants. During the course of straining, the positions of the atoms in the simulation cell are equilibrated in a microcanonical (NVE) ensemble coupled with a Langevin thermostat, which keeps the temperature at 298 K. Once the elastic constants are determined, the Voigt–Reuss–Hill (VRH) elastic properties of thaumasite are estimated following the method described in our previous studies.^{28,29} The ReaxFF calculated elastic properties are then compared with those available in the literature.

Evaluation of Stress–Strain Response. The equilibrated simulation cell of thaumasite is subjected to a range of uniaxial tensile strains along each of the three orthogonal x , y and z directions. During the infinitesimal deformation, a constant strain rate (i.e., 0.0005, 0.001, 0.005, and 0.01 ps^{-1}) is applied to the simulation cell. The atoms in the simulation cell are then fully relaxed to fit within new dimensions. It must be noted that the directions perpendicular to the one under external strain are allowed to relax anisotropically in order to capture the material's Poisson ratio. This can be achieved by using the NPT ensemble equations of motion with NULL pressure in the deformation direction and 1.0 atm pressure in the other two directions. The evolution of atomic stress in the molecular structure is recorded as a function of strain. The cell stress fluctuations induced by kinetic contributions are smeared by averaging the atomic stresses over a short time interval of 100 time steps. The straining procedure is repeated for all three Cartesian axes (x , y , and z) and continues until the maximum target strain of 25% is reached. The full set of stress and strain data are then used

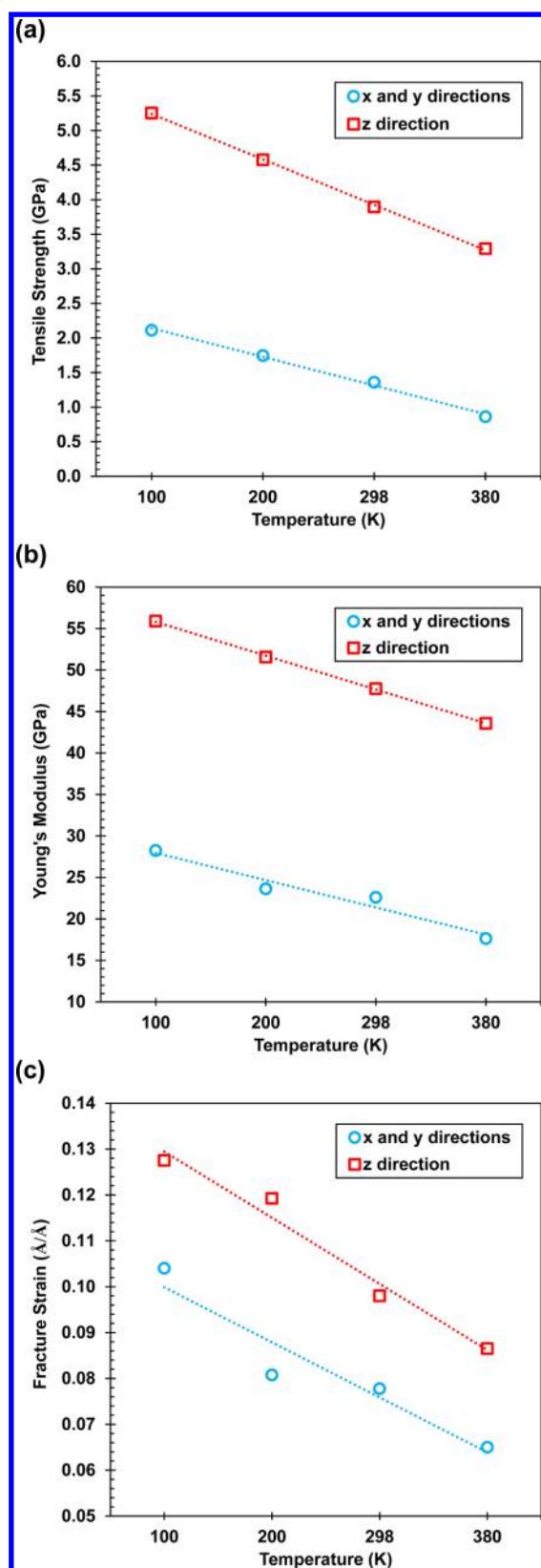


Figure 6. Mechanical properties of thaumasite at different temperatures under uniaxial tensile strains in the x/y and z directions: (a) tensile strength, (b) Young's modulus, and (c) fracture strain.

to generate the stress–strain curves for each strain direction. To examine the stress–strain behavior, 1000 strained conformers are recorded at equal intervals of the full strain range for further

chemical bond and structural damage analyses. The chemical bond analysis is used to fully characterize the structural response of thaumasite under uniaxial strain.

3. RESULTS AND DISCUSSION

Structural Characteristics of Thaumasite. The cell parameters of thaumasite equilibrated over the course of 100 ps NPT-RMD at ambient temperature and pressure are reported in Table 1. The calculated unit cell parameters accurately reproduce the experimental values with a difference less than 4% for all cases. In addition to ambient temperature (298 K) equilibration, the cell parameters of thaumasite are further investigated at different temperatures. Because thaumasite dehydrates at temperatures above 380 K,³⁰ the range of temperature considered in this study is 100–380 K. Figure 2 illustrates the volume and unit cell parameters of thaumasite at different temperatures within the established range. It can be observed that the thermal expansion of the a - and b -axis directions are very different from that of the c -axis direction. While the volume and a - and b -axis parameters expand by 2.38 and 1.19%, respectively, as the temperature increases from 100 to 380 K, the c -axis parameters remain relatively unchanged. This is primarily due to the fact that thaumasite has strong ionic–covalent $[\text{Ca}_3\text{Si}(\text{OH})_6 \cdot 12\text{H}_2\text{O}]^{4+}$ columns along the c -axis direction. The main intercolumn supports in the a - and b -axis directions are the hydrogen bonds to the sulfate and carbonate groups, which expand with increasing temperature. However, the strong nature of Ca–O and Si–O bonds resist the temperature-induced expansion in the c -axis direction. Table 2 summarizes the mean thermal expansion coefficients of thaumasite within the temperature range considered in this study. The thermal expansion coefficient of thaumasite parallel to the columnar structures is relatively constant and, in some cases negative when compared to that of the transverse direction. This can be attributed to the negative thermal expansion of the silicate octahedra, observed in the past experimental tests.⁹ The thermal expansion coefficients of thaumasite change linearly over the temperature range of 100–380 K, which is consistent with the findings of Martucci and Cruciani.¹⁰

Mechanical Properties of Thaumasite. Mechanical properties of thaumasite, including those associated with the elastic and plastic ranges, are presented and discussed in this section. Table 3 lists the elastic constants as well as the VRH elastic properties of thaumasite computed from the RMD simulations along with those obtained using Brillouin spectroscopy.¹² It can be seen that the results from the NVT-RMD simulations are consistent with those reported in the literature. As expected, it is noted that C_{33} is slightly smaller than C_{11} . This is because the strong covalent bonds that exist in the $[\text{Ca}_3\text{Si}(\text{OH})_6 \cdot 12\text{H}_2\text{O}]^{4+}$ columns result in a higher stiffness in the a – b plane. This is similar to the behavior observed for the thermal expansion of thaumasite.

The direction sensitivity of the mechanical properties of thaumasite is further investigated by analyzing the full stress–strain curves in different directions. The simulated stress–strain curves of thaumasite under uniaxial tensile strains in the x/y and z directions at ambient temperature and pressure conditions are shown in Figure 3. Although thaumasite in the x/y directions is slightly more ductile than that in the z direction, the stress–strain curves indicate that no noticeable plastic deformation takes place before the stress abruptly drops once the ultimate strength is reached. This confirms the brittle

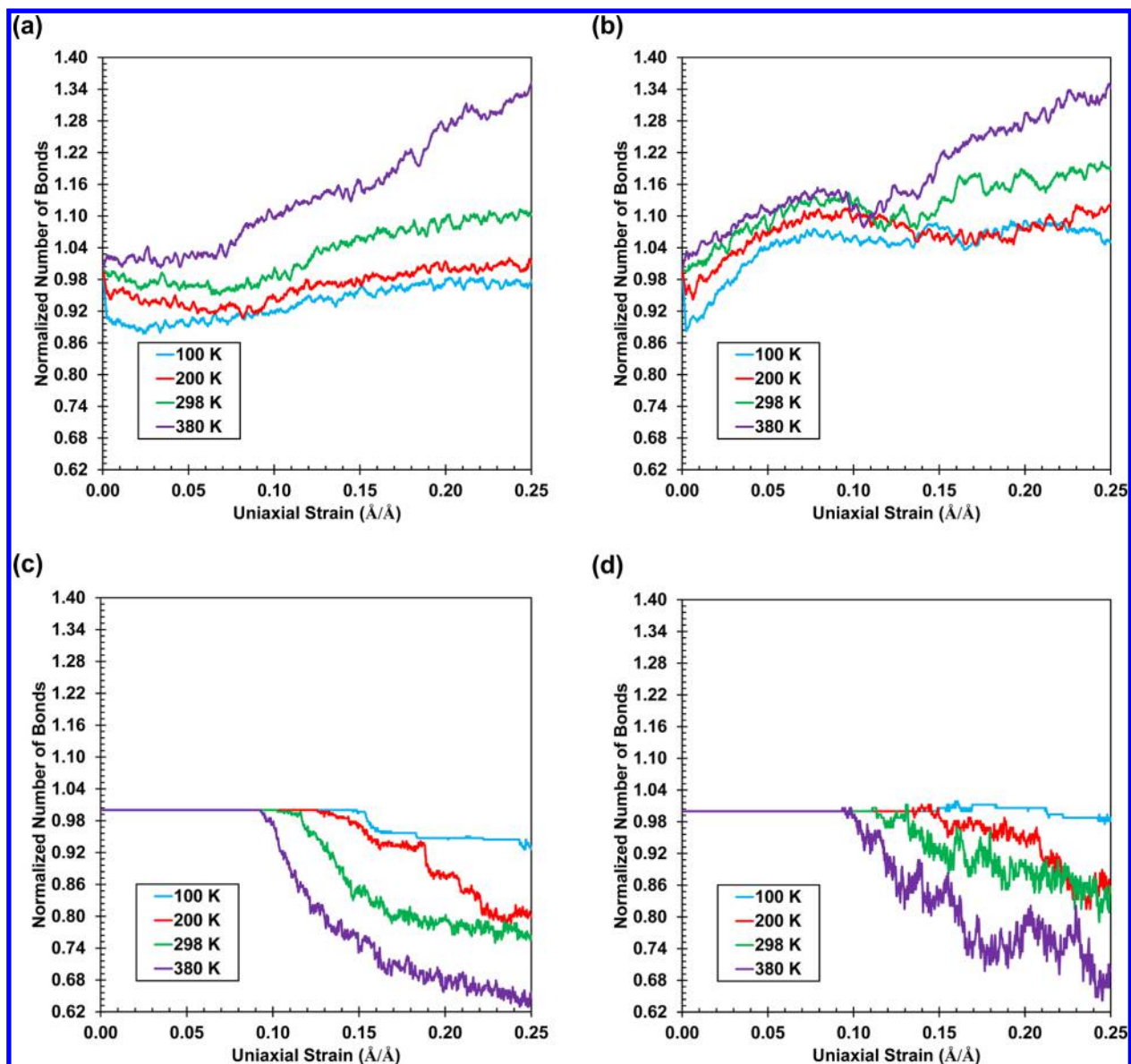


Figure 7. Changes in the number of bonds during the straining of thaumasite in different directions with various temperatures: (a) Ca–O bonds in the x/y directions, (b) Ca–O bonds in the z direction, (c) Si–O bonds in the z direction, and (d) C–O bonds in the z direction.

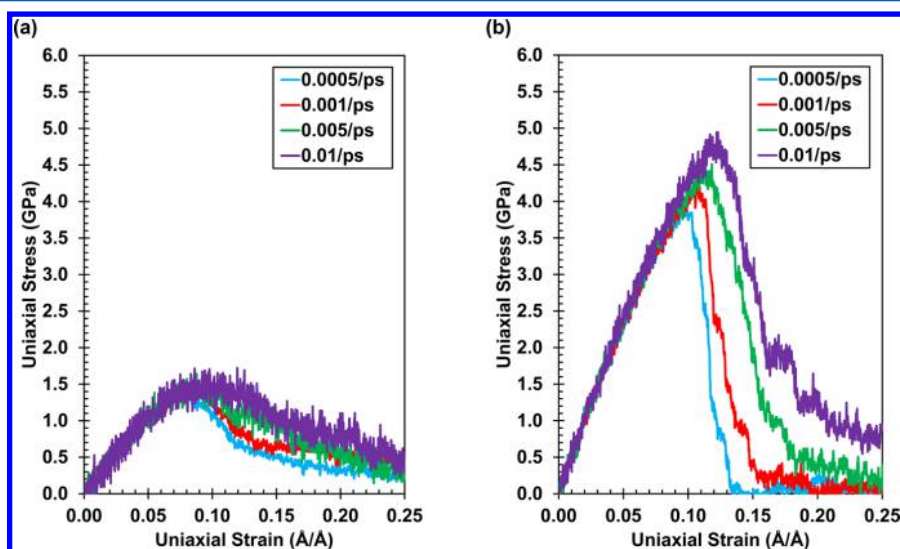


Figure 8. Stress–strain curves of thaumasite at different strain rates under uniaxial tensile strains in the (a) x/y directions and (b) z direction.

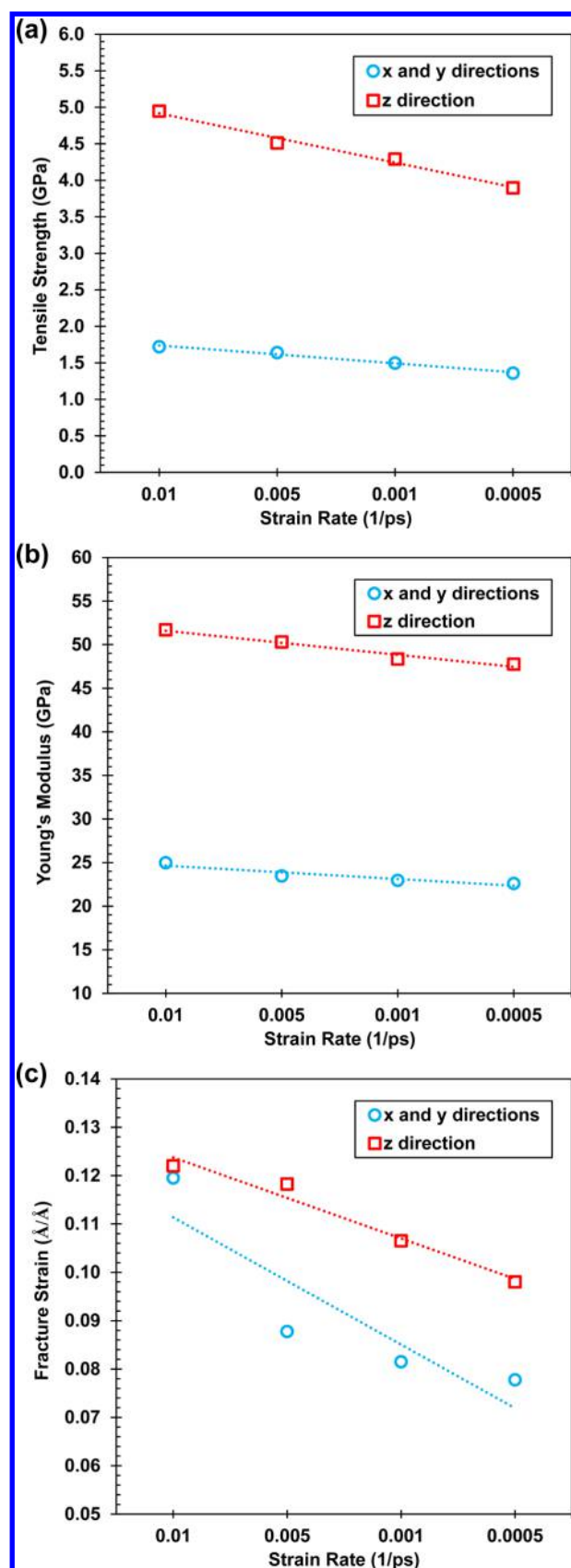


Figure 9. Mechanical properties of thaumasite under uniaxial tensile strains with various strain rates in the x/y and z directions: (a) tensile strength, (b) Young's modulus, and (c) fracture strain.

nature of structural response of thaumasite under tensile strain. While the stress–strain curves of thaumasite in the x/y and z directions have similar trends, there is a significant difference in the magnitude of the peak stress, often called ultimate strength, as well as the fracture strain. In the x/y directions, an ultimate strength of 1.36 GPa is reached at a strain of 7.8%, while in the z direction, an ultimate strength of 3.89 GPa is obtained at a strain of 9.8%. This highlights that thaumasite is almost three times stronger in the z direction than that in the x/y directions.

The stress–strain behavior observed in different directions can be further justified using chemical bond analysis. Figure 4 shows the changes in the normalized number of Ca–O, Si–O, S–O, C–O, and H–O bonds as a function of applied tensile strain in the x/y and z directions. In the x/y directions, the number of covalent Ca–O bonds decreases by increasing the applied tensile strain and increases when the minimum value is reached. This behavior is very consistent with the stress–strain curve obtained for thaumasite in the x/y directions. Contrary to Ca–O, the number of S–O, Si–O, and C–O bonds remains unchanged over the course of tensile straining until the structure collapses at a strain of 19%. This indicates that the Si–O, S–O, and C–O bonds do not have a significant contribution to the tensile strength of thaumasite in the x/y directions. On the other hand, in the z direction, the number of Ca–O, Si–O, S–O, and C–O bonds varies significantly. The z axis is parallel to the direction of the strong $[\text{Ca}_3\text{Si}(\text{OH})_6 \cdot 12\text{H}_2\text{O}]^{4+}$ columns, which are connected to the sulfate and carbonate groups with an extensive network of hydrogen bonding. This leads to the higher strength of thaumasite in the z direction.

Effect of Temperature Change on Mechanical Properties of Thaumasite. At any nonzero temperature and under no external forces, atoms in a solid still move due to thermal oscillations around equilibrium positions. Therefore, temperature is an important factor in evaluating the mechanical properties of materials given that vibrations lead to variations in bond strength. Here, separate sets of RMD simulations are performed to capture the sensitivity of the mechanical properties of thaumasite to temperature changes. The stress–strain curves of thaumasite under uniaxial tensile strains at different temperatures ranging from 100 to 380 K are shown in Figure 5. It can be seen that temperature exerts a substantial effect on the mechanical properties of thaumasite. With an increase in temperature, the tensile strength, Young's modulus, and fracture strain of thaumasite decrease significantly (Figure 6). This behavior, which is referred to as the thermal-softening effect, has been captured for a variety of materials, such as platinum nanowire,³¹ silica glass,³² polymer,³³ silicene,³⁴ and calcium hydroxide,³⁵ to name a few. By increasing the temperature from 100 to 380 K, the tensile strength, Young's modulus, and tensile strain of thaumasite drop by approximately 59.2, 37.5, and 37.5% in the x/y directions, respectively, and by 37.4, 22.0, and 32.1% in the z direction, respectively. Higher temperatures lead to an increase in the internal energy and entropy of bonds, both of which contribute to the bond structures with lower than equilibrium bond orders. Moreover, because the equilibrium length of bonds is larger at higher temperatures, the bonds can faster reach their breaking length during the tensile straining process (Figure 7). As a result, the mechanical properties of thaumasite decrease drastically with increasing temperature.

Effect of Strain Rate on Mechanical Properties of Thaumasite. According to the kinetic theory of solid fracture, the strain rate may significantly affect the mechanical properties

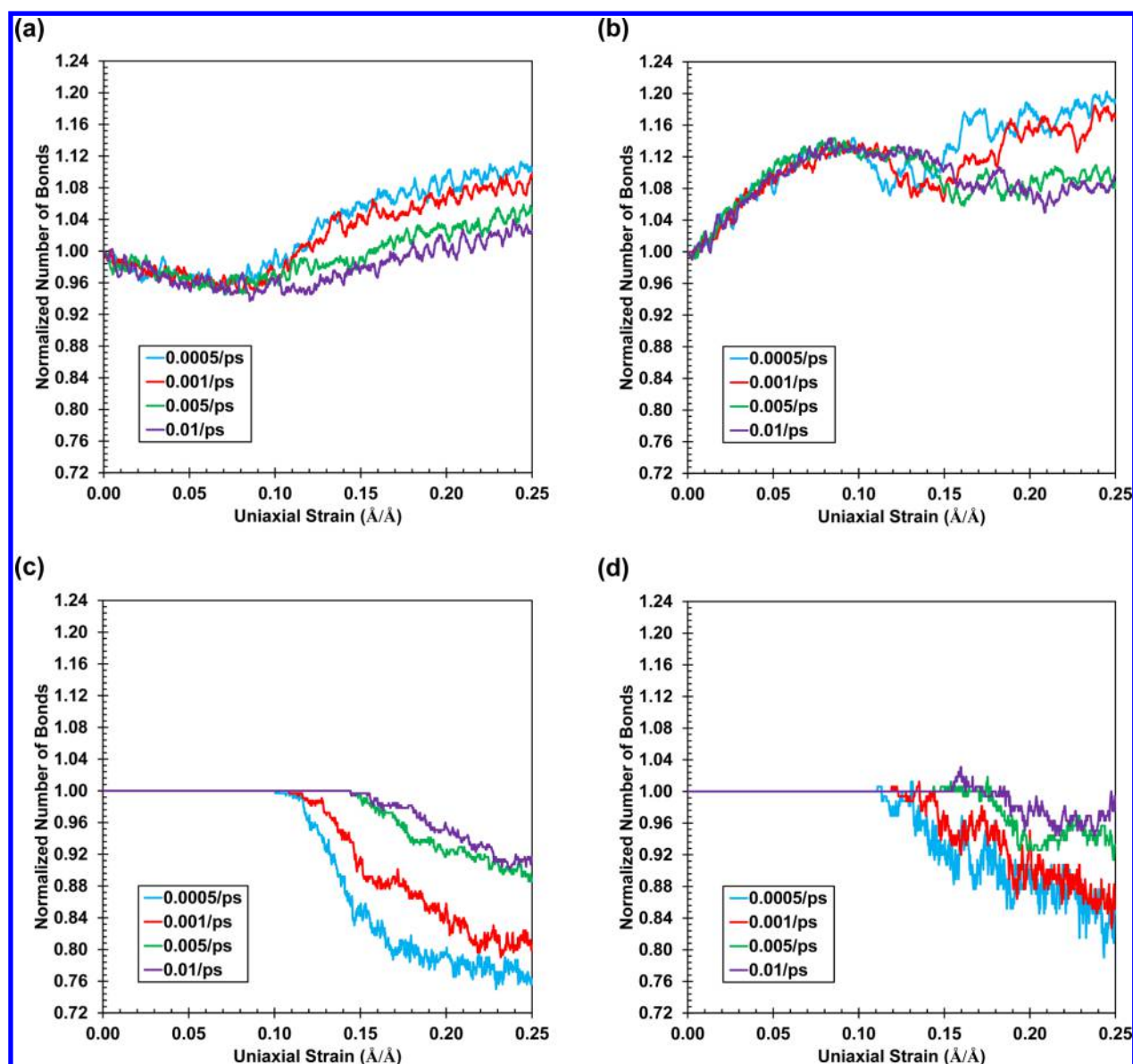


Figure 10. Changes in the number of bonds during the straining of thaumasite in different directions with various strain rates: (a) Ca–O bonds in the x/y directions, (b) Ca–O bonds in the z direction, (c) Si–O bonds in the z direction, and (d) C–O bonds in the z direction.

of solids.³⁶ To capture the effect of strain rate on the mechanical properties of thaumasite, a number of strain rates ranging from 0.0005 to 0.01 ps^{-1} are chosen. This range is within those reported in previous atomistic simulations associated with the mechanical characterization of materials.^{31,32,34,37} It must be noted that the selected strain rates are approximately 3 orders of magnitude faster than the dynamic or shock loads accessible through conventional experiments.³⁸ The short integration time steps in molecular dynamics simulations (0.25 fs in this study) as well as the computational cost of calculating the interatomic forces enforce such limits on the strain rate. Figure 8 shows the stress–strain curves of thaumasite at different strain rates under uniaxial tensile strains at ambient temperature (298 K). The ultimate strength of thaumasite (and the proportionality limit) slightly increases with increasing the strain rate, while the modulus of elasticity seems to be independent of the strain rate. By decreasing the strain rate from 0.01 to 0.0005 ps^{-1} , the ultimate strength of thaumasite drops from 4.94 to 3.89 GPa in the z direction and from 1.72 to 1.36 GPa in the x/y directions.

A similar trend is captured for the fracture strain of thaumasite (Figure 9). The fact that a lower strain rate results in reduced mechanical strength has been demonstrated via macroscopic experiments for cementitious materials.³⁹ Lower strain rates tend to increase the effect of thermal fluctuations that promote bond dissociation. Figure 10 confirms this postulate by showing the change in the number of chemical bonds in thaumasite strained with different rates. As the strain rate decreases, the dissociation rate of bonds increases. Moreover, Figure 8 shows that at higher strain rates a complete fracture requires a larger strain. This can also be inferred from the chemical bond analysis shown in Figure 10, which highlights that as the strain rate increases, a larger strain is needed for bonds to break. In other words, fast mechanical loading may reduce the probability of fracture.

4. CONCLUSIONS

The mechanical properties of thaumasite were fully characterized in this study for the first time using RMD simulations.

The simulation results showed that the stress–strain relationships of thaumasite are substantially dependent on the direction of the applied strain. Thaumasite was found to be three times stronger in the z direction than that in the x/y directions. This was because of the contribution of strong $[\text{Ca}_3\text{Si}(\text{OH})_6 \cdot 12\text{H}_2\text{O}]^{4+}$ columns that exist in the z direction. Bond analysis revealed that in the x/y directions Ca–O bonds are the only bonds that resist tensile deformations. In the z direction, however, the contribution of Si–O, S–O, and C–O bonds must be recognized as well. This properly explains the significant difference observed in the mechanical strength of thaumasite in the three orthogonal directions. The effects of temperature change and strain rate on the mechanical properties of thaumasite were also investigated in detail. As the temperature increases, the rate of chemical bond dissociation increases, which in turn results in a substantial reduction in the mechanical strength of thaumasite. On the other hand, a decrease in the strain rate favors larger atomic fluctuations accompanied by temperature-induced rearrangements, which caused a noticeable reduction in the mechanical strength of thaumasite.

AUTHOR INFORMATION

Corresponding Authors

*E-mail: shafei@iastate.edu (B.S.).

*E-mail: ajaramil@caltech.edu (A.J.-B.).

ORCID

Behrouz Shafei: 0000-0001-5677-6324

Tao Cheng: 0000-0003-4830-177X

Notes

The authors declare no competing financial interest.

ACKNOWLEDGMENTS

The Extreme Science and Engineering Discovery Environment (XSEDE), which is supported by National Science Foundation Grant Number ACI-1548562, was used for part of the atomistic simulations conducted in this study.

REFERENCES

- (1) Crammond, N. J. Thaumasite in Failed Cement Mortars and Renders from Exposed Brickwork. *Cem. Concr. Res.* **1985**, *15*, 1039–1050.
- (2) Santhanam, M.; Cohen, M. D.; Olek, J. Mechanism of Sulfate Attack: a Fresh Look Part 1: Summary of Experimental Results. *Cem. Concr. Res.* **2002**, *32*, 915–921.
- (3) Santhanam, M.; Cohen, M. D.; Olek, J. Mechanism of Sulfate Attack: a Fresh Look Part 2. Proposed Mechanisms. *Cem. Concr. Res.* **2003**, *33*, 341–346.
- (4) Neville, A. The Confused World of Sulfate Attack on Concrete. *Cem. Concr. Res.* **2004**, *34*, 1275–1296.
- (5) Crammond, N. J. The Occurrence of Thaumasite in Modern Construction—A Review. *Cem. Concr. Compos.* **2002**, *24*, 393–402.
- (6) Glasser, F. P.; Marchand, J.; Samson, E. Durability of Concrete-Degradation Phenomena Involving Detrimental Chemical Reactions. *Cem. Concr. Res.* **2008**, *38*, 226–246.
- (7) Bensted, J. Thaumasite-Background and Nature in Deterioration of Cements, Mortars and Concretes. *Cem. Concr. Compos.* **1999**, *21*, 117–121.
- (8) Bickley, J. A. The Repair of Arctic Structures Damaged by Thaumasite. *Cem. Concr. Compos.* **1999**, *21*, 155–158.
- (9) Jacobsen, S. D.; Smyth, J. R.; Swope, R. J. Thermal Expansion of Hydrated Six-Coordinate Silicon in Thaumasite, $\text{Ca}_3\text{Si}(\text{OH})_6(\text{CO}_3)(\text{SO}_4) \cdot 12\text{H}_2\text{O}$. *Phys. Chem. Miner.* **2003**, *30*, 321–329.
- (10) Martucci, A.; Cruciani, G. In Situ Time Resolved Synchrotron Powder Diffraction Study of Thaumasite. *Phys. Chem. Miner.* **2006**, *33*, 723–731.
- (11) Gatta, G. D.; McIntyre, G. J.; Swanson, J. G.; Jacobsen, S. D. Minerals in Cement Chemistry: A Single-Crystal Neutron Diffraction and Raman Spectroscopic Study of Thaumasite, $\text{Ca}_3\text{Si}(\text{OH})_6(\text{CO}_3)(\text{SO}_4) \cdot 12\text{H}_2\text{O}$. *Am. Mineral.* **2012**, *97*, 1060–1069.
- (12) Scholtzová, E.; Tunega, D.; Speziale, S. Mechanical Properties of Ettringite and Thaumasite-DFT and Experimental Study. *Cem. Concr. Res.* **2015**, *77*, 9–15.
- (13) Liu, L.; Jaramillo-Botero, A.; Goddard, W. A., III; Sun, H. Development of a ReaxFF Reactive Force Field for Ettringite and Study of its Mechanical Failure Modes from Reactive Molecular Dynamics. *J. Phys. Chem. A* **2012**, *116*, 3918–3925.
- (14) Hajilar, S.; Shafei, B. Mechanical Failure Mechanisms of Hydrated Products of Tricalcium Aluminate: A Reactive Molecular Dynamics Study. *Mater. Des.* **2016**, *90*, 165–176.
- (15) Van Duin, A. C. T.; Dasgupta, S.; Lorant, F.; Goddard, W. A., III ReaxFF: A Reactive Force Field for Hydrocarbons. *J. Phys. Chem. A* **2001**, *105*, 9396–9409.
- (16) Jaramillo-Botero, A.; Cheng, T.; Liu, L.; Goddard, W. A., III First-Principles Based Modeling of Cement Hydration Kinetics and Dynamics; Nanomechanics for Structural Materials Meeting (DOT Award No. DTFH61-10-C-00019); DOT Turner-Fairbank Highway Research Center, VA, March 6, 2014.
- (17) Jaramillo-Botero, A.; Naserifar, S.; Goddard, W. A., III A General Multi-Objective Force Field Optimization Framework, with Application to Reactive Force Fields for Silicon Carbide. *J. Chem. Theory Comput.* **2014**, *10*, 1426–1439.
- (18) Edge, R. A.; Taylor, H. F. W. Crystal Structure of Thaumasite, $[\text{Ca}_3\text{Si}(\text{OH})_6 \cdot 12\text{H}_2\text{O}](\text{SO}_4)(\text{CO}_3)$. *Acta Crystallogr., Sect. B: Struct. Crystallogr. Cryst. Chem.* **1971**, *27*, 594–601.
- (19) Effenberger, H.; Kirfel, A.; Will, G.; Zobetz, E. A Further Refinement of the Crystal Structure of Thaumasite, $\text{Ca}_3\text{Si}(\text{OH})_6\text{CO}_3\text{SO}_4 \cdot 12\text{H}_2\text{O}$. *Neus Jahrbuch für Mineralogie Monatshefte* **1983**, *2*, 60–68.
- (20) Moenke, H. Ein Weiteres Mineral mit Silizium in 6er-Koordination: Thaumasit. *Naturwissenschaften* **1964**, *51*, 239.
- (21) Grimmer, A. R.; Wieker, W.; Lampe, F.; Fechner, E.; Peter, R.; Molgedey, G. Hochauflösende ^{29}Si -NMR an Festen Silicaten: Anisotropie der Chemischen Verschiebung im Thaumasite. *Z. Chem.* **1980**, *20*, 453.
- (22) Stebbins, J. F.; Kanzaki, M. Local Structure and Chemical Shifts for Six-Coordinated Silicon in High-Pressure Mantle Phases. *Science* **1991**, *251*, 294–298.
- (23) Yang, H.; Prewitt, C. T.; Frost, D. J. Crystal Structure of Dense Hydrous Magnesium Silicate, Phase D. *Am. Mineral.* **1997**, *82*, 651–654.
- (24) Frost, D. J.; Fei, Y. Stability of Phase D at High Pressure and High Temperature. *J. Geophys. Res.* **1998**, *103*, 7463–7474.
- (25) Wunder, B.; Jahn, S.; Koch-Müller, M.; Speziale, S. The 3.65 Å Phase, $\text{MgSi}(\text{OH})_6$: Structural Insights from DFT-Calculations and T-Dependent IR Spectroscopy. *Am. Mineral.* **2012**, *97*, 1043–1048.
- (26) Plimpton, S. Fast Parallel Algorithms for Short-Range Molecular Dynamics. *J. Comput. Phys.* **1995**, *117*, 1–19.
- (27) Rappe, A. K.; Goddard, W. A., III Charge Equilibration for Molecular Dynamics Simulations. *J. Phys. Chem.* **1991**, *95*, 3358–3363.
- (28) Hajilar, S.; Shafei, B. Nano-Scale Characterization of Elastic Properties of AFt and AFm Phases of Hydrated Cement Paste. *Proceedings of the European Conference on Computational Modeling of Concrete Structures (EURO-C)*; St. Anton am Arlberg: Austria, 2014; Vol. 1, pp 299–306.
- (29) Hajilar, S.; Shafei, B. Nano-Scale Investigation of Elastic Properties of Hydrated Cement Paste Constituents using Molecular Dynamics Simulations. *Comput. Mater. Sci.* **2015**, *101*, 216–226.
- (30) Brough, A. R.; Atkinson, A. Micro-Raman Spectroscopy of Thaumasite. *Cem. Concr. Res.* **2001**, *31*, 421–424.
- (31) Koh, S. J. A.; Lee, H. P.; Lu, C.; Cheng, Q. H. Molecular Dynamics Simulation of a Solid Platinum Nanowire under Uniaxial

Tensile Strain: Temperature and Strain-Rate Effects. *Phys. Rev. B: Condens. Matter Mater. Phys.* **2005**, *72*, 085414.

(32) Pedone, A.; Malavasi, G.; Menziani, M. C.; Segre, U.; Cormack, A. N. Molecular Dynamics Studies of Stress-Strain Behavior of Silica Glass under a Tensile Load. *Chem. Mater.* **2008**, *20*, 4356–4366.

(33) Li, C.; Strachan, A. Molecular Dynamics Predictions of Thermal and Mechanical Properties of Thermoset Polymer EPON862/DETDA. *Polymer* **2011**, *52*, 2920–2928.

(34) Pei, Q. X.; Sha, Z. D.; Zhang, Y. Y.; Zhang, Y. W. Effects of Temperature and Strain Rate on the Mechanical Properties of Silicene. *J. Appl. Phys.* **2014**, *115*, 023519.

(35) Hajilar, S.; Shafei, B. Assessment of Structural, Thermal, and Mechanical Properties of Portlandite through Molecular Dynamics Simulations. *J. Solid State Chem.* **2016**, *244*, 164–174.

(36) Xiao, T.; Ren, Y.; Liao, K. A Kinetic Model for Time-Dependent Fracture of Carbon Nanotubes. *Nano Lett.* **2004**, *4*, 1139–1142.

(37) Wu, X.; Moon, R. J.; Martini, A. Tensile Strength of $I\beta$ Crystalline Cellulose Predicted by Molecular Dynamics Simulation. *Cellulose* **2014**, *21*, 2233–2245.

(38) Zhuang, S.; Lu, J.; Ravichandran, G. Shock Wave Response of a Zirconium-Based Bulk Metallic Glass and its Composite. *Appl. Phys. Lett.* **2002**, *80*, 4522.

(39) Rossi, P. Strain Rate Effects in Concrete Structures: the LCPC Experience. *Mater. Constr.* **1997**, *30*, 54–62.